# Steric and Electronic Effects in Methyl-Substituted 2,2′-Bipyrroles and Poly(2,2′-Bipyrrole)s: Part II. Theoretical Investigation on Monomers

Carlo Gatti,*,† and Giovanni Frigerio

*Centro CNR per lo Studio delle Relazioni fra Struttura e Reattività Chimica, via C. Golgi 19, 20133 Milano, Italy*

Tiziana Benincori,‖ Elisabetta Brenna, and Franco Sannicolò*,‡

*Dipartimento di Chimica Organica e Industriale dell'Università e Centro CNR Sintesi e Stereochimica Speciali Sistemi Organici, via C. Golgi 19, 20133 Milano, Italy*

Gianni Zotti,*,§ Sandro Zecchin, and Gilberto Schiavon

*Istituto di Polarografia ed Elettrochimica Preparativa, Consiglio Nazionale delle Ricerche, c.so Stati Uniti 4, 35020 Padova, Italy*

*Received February 1, 2000. Revised Manuscript Received March 2, 2000*

The effects of *N*- and $C_\beta$-methyl substitution in pyrrole and 2,2′-bipyrrole were investigated through ab initio calculations and Atoms in Molecules analysis of the resulting wave functions. Replacement of a hydrogen atom with a methyl group in pyrroles lowers the ionization potential, with substitution at C3 being more efficient than N-substitution because of the larger release of $\pi$ population to the ring in the former case. Full geometry optimization at RHF/6-31G** level and as a function of the torsion angle $\tau$ between two adjacent rings demonstrates that the increasing loss of planarity in the 2,2′-bipyrrole, *N*,*N*′-dimethyl-2,2′-bipyrrole, and 3,3′-dimethyl-2,2′-bipyrrole series, adversely affects the positive contributions expected from methyl substitution. An intramolecular interaction energy model shows that the greater anti-planarization energy of *N*,*N*′-dimethyl-2,2′-bipyrrole, as compared to 3,3′-dimethyl-2,2′-bipyrrole, is due to the larger decrease in the stabilizing electrostatic term and to the larger increase in the destabilizing nonbonding contribution which occurs at $\tau = 0°$ in the former. Calculations on the corresponding monocations and analysis of new conductivity measures on substituted poly(2,2′-bipyrrole)s suggest that the ease in achieving local chain planarity in doped polypyrroles should be more closely correlated to the anti-planarization energies of the charged monomers rather than to anti-planarization energies of the neutral monomers.

## Introduction

Solubility and improved processability of conducting polyheterocycles is generally attained by introduction of alkyl substituents on the monomer. Chemical and electrochemical polymerization of a great variety of 3-alkylthiophenes[1] and bithiophenes[2] gives materials showing greater solubility and higher conductivity than the unsubstituted polythiophene. The same strategy, when applied to polypyrroles by alkylating either the nitrogen atom or the $\beta$-carbon atom of the starting pyrrole monomer, produces contrasting results.

N-Alkylation affords in general scarcely conductive materials,[3,4] while 3-alkyl substitution of pyrrole involves such a troublesome synthetic sequence that only a few reports have been published[5−10] on poly(3-alkylpyrrole)s. Yet these latter materials were found to be much more conductive (2−10 S cm$^{-1}$) than the corresponding N-substituted polymers ($10^{-3}$ S cm$^{-1}$)[3,4] and even better (270 S cm$^{-1}$)[7] than polypyrrole itself (100 S cm$^{-1}$),[11] when prepared under specially selected, optimized conditions.

† E-mail address: c.gatti@csrsrc.mi.cnr.it.
‡ E-mail address: staclaus@icil64.cilea.it.
§ E-mail address: gzotti@pdadr1.pd.cnr.it.
‖ New address: Dipartimento di Scienze Chimiche, Fisiche e Matematiche dell' Università dell' Insubria, Via Lucini, 3-22100 COMO

(1) Roncali, J. *Chem. Rev*. **1992**, *92*, 711.
(2) Souto Maior, R. M.; Hinkelmann, K.; Eckert, H.; Wudl, F. *Macromolecules* **1990**, *23*, 1268. Zagorska, M.; Krische, B. *Polymer* **1990**, *31*, 1379. Arbizzani, C.; Barbarella, G.; Bongini, A.; Mastragostino, M.; Zambianchi, M. *Synth. Met*. **1992**, *52*, 329.
(3) Diaz, A. F.; Castillo, J.; Kanazawa, K. K.; Logan, J. A. *J. Electroanal. Chem*. **1982**, *133*, 233.
(4) Diaz, A. F.; Castillo, J. I.; Logan, J. A.; Lee, W.-Y. *J. Electroanal. Chem*. **1981**, *129*, 115.
(5) Ruhe, J.; Ezquerra, T.; Wegner, G. *Makromol. Chem. Rapid Comm*. **1989**, *10*, 103.
(6) Masuda, H.; Tanaka, S.; Kaeriyama, K. *J. Chem. Soc. Chem. Comm*. **1989**, 725.
(7) Kaeriyama, K.; Sato, M.; Hamada, K. *Makromol. Chem. Rapid Comm*. **1989**, *10*, 171.
(8) Delabouglise, D.; Roncali, J.; Lemaire, M.; Garnier, F. *J. Chem. Soc. Chem. Commun*. **1989**, 475.
(9) Kaeriyama, K.; Tanaka, S.; Sato, M.-A.;.Hamada, K. *Synth. Met*. **1989**, *28*, C611.
(10) Salmon, M.; Diaz, A. F.; Logan, A. J.; Krounbi, M.; Bargon, J. *Mol. Cryst. Liq. Cryst*. **1982**, *83*, 265.
(11) Wynne, K. J.; Street, G. B. *Macromolecules* **1985**, *18*, 2361.

10.1021/cm000092r CCC: $19.00 
Published on Web 04/22/2000

In the preceding paper,[12] the synthesis and the electrochemical polymerization of 2,2′-bipyrrole and all its possible *N*- and *C*-monomethyl and dimethyl derivatives was afforded. That paper constitutes a first part of a study aimed at a mature comprehension of the differing effects of nitrogen and $\beta$-carbon methyl substitution on the electrical properties of the resulting polymers. In particular, it has been shown that the use of monomers, which allowed us to obtain defect-free materials, and the adoption of fine-tuned, identical experimental conditions in the electrochemical anodic oxidation process yielded for the first time quite similar conductivities for *N*- and $\beta$-methyl-substituted polypyrroles. In the present paper we report, as a second part of the study, the calculation of the electronic properties of some of the synthesized monomers. Our purpose was, on one hand, to explain part of the experimental data displayed in the preceding paper[12] and, on the other hand, to reach a deeper understanding of the interplay between steric and electronic effects that are induced by *N*- and $C_\beta$-methyl substitution on the investigated monomers. Last, but not least important purpose, was to propose—on the basis of calculations on the charged monomers—a tentative explanation for the unexpected similar conductivities found for *N*- and $C_\beta$-methyl-substituted polypyrroles in the first part of our study.

Calculations on oligomers representative of polyaromatic materials have been already published in the last years.[13−15] These investigations were mainly focused on the evolution—as the torsion angle $\tau$ between adjacent rings increases—of electronic properties of interest in the conducting polymer area. In particular, Brédas et al.[14] obtained a clear picture of how significantly the positive contributions to the electronic properties expected from substituents can be adversely affected by the loss of planarity. They studied a number of $\pi$-conjugated biheteroaromatic compounds, including bipyrrole, 3,3′-dimethyl-2,2′-bipyrrole, and 1,1′-dimethyl-2,2′-bipyrrole and found that the evolution of the electronic properties, especially ionization potential and band gap, is adequately fitted by a cosine function, as is the related decrease of the overlap between the $\pi$ orbitals on adjacent rings for increasing $\tau$ angles. Thus, substituents which do not cause torsion angles greater than about 40° along the chains were thought[14] to be generally quite acceptable, since such a torsion induces only a slight effect on the electronic properties of the polymers. Yet, Brédas et al.[14,16] also pointed out that the possibility of achieving a coplanar conformation after doping might be of great importance for the intrachain mobility of charge defects such as polarons or bipolarons. So, not only the value of the torsion angle corresponding to the minimum energy conformation was found to be significant for achieving high conductivity, but even more so the planarization barrier height.

**Scheme 1**

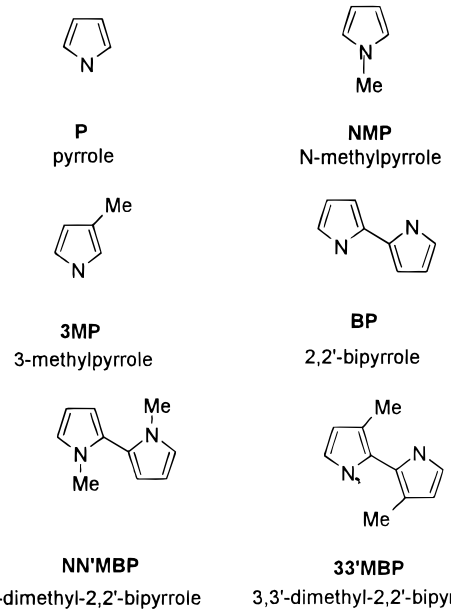


Although the reported conclusions of Brédas et al.[14] were enlightening, far-reaching, and based on systems that largely overlap with ours, the following considerations should substantiate this theoretical (re)investigation. First, the present-day enhanced computational facilities permit full geometrical optimizations at Hartree−Fock level with a good quality basis set—something that was not reasonably feasible 15 years ago on such large systems—and, second, the adoption of the Quantum Theory of Atoms in Molecules[17,18] approach for analyzing their computed wave functions should lead to an improved understanding of the interplay between electronic and steric effects in these systems.

**Ab Initio Computations.** The list of investigated systems, along with the shorthand notation used throughout the paper is reported in Scheme 1. The geometry of all systems was fully optimized at the Restricted Hartree−Fock (RHF) 6-31G**(5D) level,[19] and using the following geometrical constraints: $C_{2v}$ for pyrrole, $C_s$ and $C_1$ for the *N*- and 3-methyl-substituted pyrroles, respectively, and $C_2$ for all the remaining systems. In the case of bipyrroles, constrained $C_2$ geometry optimizations were also performed at fixed values of the torsion angle $\tau$, by varying $\tau$ in steps of 15°, from antiperiplanar ($\tau = 0°$) to synperiplanar ($\tau = 180°$) conformations. The influence of electron correlation effects on torsion potentials and barrier heights was checked by using the second-order Møller−Plesset (MP2) perturbation theory.[20,19] MP2 computations on the RHF/6-31G** geometries were performed at selected $\tau$ values, adopting frozen core (FC) approximation and 6-31G* basis set.[19] These computations are referred to as MP2(FC)/6-31G*//RHF/6-31G**, where the double bar means "at the geometry of".

(12) Benincori, T.; Brenna, E.; Sannicolò, F.; Zotti, G.; Zecchin, S.; Schiavon, G.; Gatti, C.; Frigerio, G. *Chem. Mater.* **2000**, *12*, 1480 (preceding paper in this issue).
(13) Brédas, J. L.; Silbey, R.; Boudreaux, D. S.; Chance, R. R. *J. Am. Chem. Soc.* **1983**, *105*, 6555. Brédas, J. L.; Heeger, A. J. *Macromolecules* **1990**, *23*, 1150.
(14) Brédas, J. L.; Street, G. B.; Thémans, B.; André, J. M. *J. Chem. Phys.* **1985**, *83*, 1323.
(15) Brédas, J. L.; Heeger, A. J. *Macromolecules* **1990**, *23*, 1150.
(16) Brédas, J. L.; Street, G. B. *Acc. Chem. Res.* **1985**, *18*, 309.
(17) Bader, R. F. W. *Atoms in Molecules. A Quantum Theory*; International Series of Monographs on Chemistry no. 22; Oxford University Press: Oxford, 1990.
(18) Bader, R.F. W. *Phys. Rev.* **1994**, *B49*, 13348.
(19) Hehre, W. J.; Radom, L.; Schleyer, P. v. R.; Pople, J. A. *Ab initio Molecular Orbital Theory*; John Wiley & Sons: New York, 1986 and references therein.
(20) Møller, C.; Plesset, M. S. *Phys. Rev.* **1934**, *46*, 618.

Ionization potentials (IP) were estimated, according to Koopmans' theorem,[21] by taking the inverse (IP = $-\epsilon_{HOMO}$) of the energy of the highest occupied molecular orbital (HOMO). These IP estimates were compared with computed vertical IPs, according to IP(M) = $\Delta E_{MP2}$(M) = $E_{ROMP2}(M^+) - E(M)_{MP2}$, where the two energies $E$ refer to the restricted open and restricted MP2 energies for the cation ($M^+$) and the neutral system (M), respectively, M being one of the studied compounds. Energies $E$ were evaluated at the RHF/6-31G** optimized geometry of M. Vertical IP(M) values were also computed using RHF for the neutral systems and either ROHF (Restricted Open Hartree−Fock) or UHF (Unrestricted Hartree−Fock) Hamiltonian for the cationic systems. These IP values are referred to as $\Delta E_{ROHF}$ and $\Delta E_{UHF}$, respectively. The $\pi-\pi^*$ transition energies were approximated by the calculated $\epsilon_{LUMO} - \epsilon_{HOMO}$ difference and compared with computed excitation energies at the configuration interaction (CI) level, using 6-31G* basis set, RHF/6-31G** geometries and only single excitations (CIS).[19] The corresponding level of theory is hereinafter referred to as CIS/6-31G*//RHF/6-31G**.

**Quantum Theory of Atoms in Molecules.** Among other properties of interest as a function of the torsion angle, intra-ring bond order $n$, bond ellipticity $\epsilon$, and overlap $P$ with neighboring intra-ring bonds were evaluated according to the Quantum Theory of Atoms in Molecules (AIM) approach. A comprehensive overview of AIM is given in ref 17, while a very condensed outline of the physical basis of this theory may be found in ref 18. Here we summarize only those points of the theory which are pertinent to our study. On the basis of quantum mechanics and on a study of the topological properties of electron density $\rho(r)$, this theory allows for a precise definition of the chemical concepts of atoms, bonds and structure. The nuclei of two bonded atoms are connected by a line—bond path—where $\rho(r)$ is maximum with respect to any lateral displacement from the line. The point $r_b$ where the density attains a minimum value along the bond path, is a critical point (a point where $\nabla\rho$ vanishes), called bond critical point (BCP). Each BCP is characterized by three eigenvalues $\lambda_i$ or *curvatures*, one positive ($\lambda_3$) and two negative ($\lambda_1$,$\lambda_2$; $\lambda_1 \leq \lambda_2$), associated with eigenvectors of the Hessian matrix of $\rho$ at $r_b$. The local properties of $\rho$ at a BCP reflect and summarize very concisely the particular type of chemical interaction occurring between the corresponding bonded atoms. The value of electron density at the BCP, $\rho(r_b)$, serves[22−24] as a measure of bond order $n$, according to the empirical relationship[22] $n = \exp\{A[\rho(r_b) - B]\}$, where $A$ and $B$ depend on the calculation model adopted (carbon−carbon bond: $A = 6.518$ Å$^3$, $B = 0.253$ Å$^{-3}$; nitrogen−carbon bond: $A = 5.237$ Å$^3$, $B = 0.278$ Å$^{-3}$; RHF/6-31G** model).[25] The two negative curvatures of a BCP, associated with eigenvectors defining a surface perpendicular to the bond path at the BCP, give the bond ellipticity $\epsilon = [(\lambda_1/\lambda_2) - 1]$, a measure of the extent to which charge is preferentially accumulated in a given plane. The axis associated with $\lambda_2$ defines the major axis of the elliptical contour of $\rho$ around the bond axis. For the carbon−carbon bond in ethane, $\lambda_1$ and $\lambda_2$ are obviously degenerate and ellipticity is zero; in conjugated systems, like substituted bipyrroles, the intra- and interannular carbon−carbon bonds should exhibit ellipticity values different from zero and associated major axes pointing in a direction approximately coincident with that of the maximum in $\pi$ distribution of the usual molecular orbital theory. The overlap of the major axes of neighboring bonds $i-j$ and $j-k$, calculated as the dot product of the associated eigenvectors and hereinafter referred to as $O_{ijk}$, gives the extent of charge delocalization in noncoplanar conjugated systems.[26]

**Intramolecular Interaction Energy.** As an aid in interpreting the minimum energy conformations adopted by bipyrroles, depending on their methyl-substitution, the interaction energy $E_{int}$ between sets $\{A\}$ and $\{B\}$ of facing atoms in the two pyrrole rings, was evaluated. $E_{int}$ was estimated as a sum of atom−atom electrostatic ($E^{ij}_{es}$) and nonbonding ($E^{ij}_{nb}$) contributions

$$E_{int} = (E_{es} + E_{nb}) = \sum_{i\in\{A\}} \sum_{j\in\{B\}} (E^{ij}_{es} + E^{ij}_{nb}) \qquad (1)$$

where the generic $E^{ij}_{es}$ term is given by

$$E^{ij}_{es} = Tq^iq^j + T_\alpha(q^i\mu^j_\alpha - q^j\mu^i_\alpha) + T_{\alpha\beta}({}^1/_3q^i\Theta^j_{\alpha\beta} + {}^1/_3q^j\Theta^i_{\alpha\beta} - \mu^i_\alpha\mu^j_\beta) + {}^1/_3T_{\alpha\beta\gamma}(\mu^i_\alpha\Theta^j_{\beta\gamma} - \mu^i_\alpha\Theta^j_{\beta\gamma}) + {}^1/_9T_{\alpha\beta\gamma\delta}\Theta^i_{\alpha\beta}\Theta^j_{\gamma\delta} + \ldots = MM_{ij} + MD_{ij} + DD_{ij} + MQ_{ij} + DQ_{ij} + QQ_{ij} + \ldots \quad (2)$$

with implicit summations over dummy Greek indices. The Cartesian tensors $T_{\alpha\beta\ldots}$ are derivatives of $T = 1/R$, so that $T_\alpha = -R_\alpha/R^3$, $T_{\alpha\beta} = (3R_\alpha R_\beta - R^2\delta_{\alpha\beta})/R^5$, etc., where **R** is the vector joining atoms $i$ and $j$ and $R$ its modulus $|\mathbf{R}|$. For each atom, the atomic net charge $q$, the atomic first moment (dipole) $\mu_\alpha$, and second moment (quadrupole) $\Theta_{\alpha\beta}$ components were evaluated by integration of the corresponding property densities over the atomic basin Ω. Within AIM approach, the latter is the portion of space including the nucleus and enclosed by the atomic surface $S$ defined by the boundary condition $\nabla\rho(\mathbf{r})\cdot\mathbf{n}(\mathbf{r}) = 0$, where $\mathbf{n}(\mathbf{r})$ is a unit vector normal to the surface at **r** and **r** denotes any point on the surface $S$. Equation 2 affords decomposition of the interaction energy between atoms $i$ and $j$ in a sum of electrostatic contributions, namely the monopole−monopole $MM_{ij}$, the monopole−dipole $MD_{ij}$, the dipole−dipole $DD_{ij}$, the monopole−quadrupole $MQ_{ij}$, the dipole−quadrupole $DQ_{ij}$, and the quadrupole−quadrupole $QQ_{ij}$ terms. Further terms were neglected in our analysis. The evaluation of $E^{ij}_{es}$ according to eq 2 was proposed long ago by Cooper et al.[27] as a tool to study *intermolecular* interactions and to predict conformations of strongly hydrogen-

(21) Koopmans, T. A. *Physica* **1933**, *1*, 104.
(22) Bader, R. F. W.; Slee, T. S.; Cremer, D.; Kraka, E. *J. Am. Chem. Soc.* **1983**, *105*, 5061.
(23) Cremer, D.; Kraka, E. *Croatica Chem. Acta* **1984**, *57*, 1259.
(24) Gatti, C.; Barzaghi, M.; Bonati, L.; Pitea, D. *Quantum Chemistry-Basic Aspects, Actual Trends*, Studies in Physical and Theoretical Chemistry **1989**, *62*, 401.
(25) The values of $A$ and $B$ parameters were determined by a least-squares method, using the same set of reference compounds, with preassigned bond orders, used in ref 23.
(26) Cremer, D.; Kraka, E.; Slee, T. S.; Bader, R. F. W.; Lau, C. D. H.; Nguyen-Dang, T. T.; MacDougall, P. J. *J. Am. Chem. Soc.* **1983**, *105*, 5069.
(27) Cooper, D. L.; Stutchbury, N. C. J. *Chem. Phys. Lett.* **1985**, *120*, 167.

bonded complexes. Such an equation is here applied to *intramolecular* interactions, a use recently exploited by Glaser et al.[28] for the interpretation of neighboring group interactions in crystal structures. The following points should be highlighted: (*i*) the molecular electron distributions of the interacting monomers are kept frozen in Cooper's model,[27] while in our case the charge distributions of interacting atoms turn out to be mutually polarized, as a result of the SCF procedure and (*ii*) short-range repulsion and long-range dispersion energies are neglected in ref 28, whereas in our model they are referred to as nonbonding energies and approximated by atom−atom potentials with parameters taken either from experiments[29,30] (and in particular from crystal data) or derived[31] from the Gordon−Kim electron gas model.[32−34] In the former case potential functions of both the Lennard-Jones (6-12) and Buckingham (6-exp) types were used with parameters taken from ref 29 and from Table 6 of ref 30, respectively. The full set of experimental parameters and potential functions adopted for the Lennard-Jones and Buckingham models is reported in ref 35. In summary, our model is formally similar to that exploited by Spackman[36] and Spackman et al.[37] for calculating the energies of molecular interactions from Bragg diffraction data, the terms $E_{es}$ and $E_{pen}$ (eq 1 of ref 36) being included in our $E_{es}$ term and the remaining terms ($E_{rep} + E_{disp}$) being similarly approximated by atom−atom potentials. Again, since we are applying our model to intramolecular interactions, the polarization, induction and charge-transfer terms—neglected in Spackman's model—are here implicitly taken into account through the SCF step.

**Atomic Electron Population Partitioning.** To elucidate the charge rearrangements caused by methyl substitution in pyrroles, the AIM integrated electron atomic populations $P(\Omega)$ were partitioned in $\sigma$, $[P^{\sigma}(\Omega)]$, and $\pi$, $[P^{\pi}(\Omega)]$ contributions. This type of partitioning has been previously applied.[38−40]

**Programs.** Wave function calculations were performed with the GAUSSIAN-94 package[41] and the resulting densities analyzed with the PROAIM suite of programs.[42]

**Table 1. RHF/6-31G** and MP2/6-31G*//RHF/6-31G** Relative Energies (kcal/mol) as a Function of Torsion Angle ($\tau$) around the Inter-Ring Bond in Bipyrroles[a]**

| system | $\tau$ | RHF/6-31G** | MP2/6-31G*//RHF/6-31G** |
|---|---|---|---|
| **BP** | 0 | 0.70 | 1.30 |
| | 30 | 0.01 | 0.15 |
| | **32.8** | **0.00** | |
| | **41.2** | | **0.00** |
| | 60. | 0.89 | 0.38 |
| | 90. | 2.25 | 1.54 |
| | 180. | 3.56 | 4.29 |
| **NN′MBP** | 0 | 5.15 | 5.56 |
| | 30 | 1.40 | 1.26 |
| | **59.6** | | **0.00** |
| | 60. | 0.00 | 0.00 |
| | **60.7** | **0.00** | |
| | 90 | 0.06 | 0.15 |
| | 180 | 12.53 | 10.16 |
| **33′MBP** | 0 | 2.74 | 2.05 |
| | 30. | 0.73 | 0.47 |
| | **52.3** | | **0.00** |
| | **54.9** | **0.00** | |
| | 60 | 0.02 | 0.05 |
| | 90 | 0.52 | 0.65 |
| | 180 | 8.58 | 7.21 |

[a] All energies relative to the corresponding energy minimum, which occurs at bold $\tau$. For the sake of conciseness, only key energy points along the $\tau$ coordinate are reported.

## Calculation Results and Discussion

Table 1 lists the RHF and MP2 energies for bipyrroles, relative to their energy minimum and as a function of the torsion angle $\tau$ around the interannular bond. Only key energy points along $\tau$ are reported in the table. The whole potential curves are portrayed in Figure 1a for the RHF/6-31G** model. Evolution, as a function of $\tau$, of interannular bond lengths and orders are shown in Figure 1b,c, while the associated changes in ionization potential and interannular bond ellipticities are represented in Figure 2. Table 2 compares the theoretical vs experimental[12] vertical ionization potential (IP) and $\pi$-$\pi$* transition energies in pyrroles and bipyrroles.

**Conformations, Planarization Energies, and Interannular Bond Lengths.** Table 1 shows that bipyrroles prefer nonplanar conformations, with large values of the twisting angle $\tau$. The largest deviation from planarity occurs for **NN′MBP** ($\tau = 59.6°$, RHF/6-31G**) and the lowest one for the unsubstituted bipyrrole ($\tau = 32.8°$). The same trend is found when correlation corrections, at the MP2 level and on the RHF geometries, are introduced, though the resulting minimum energy torsion angles span in this case a somewhat narrower range (19.5 vs 26.8°). Inspection of Figure 1a shows that the **BP** curve is rather flat over the whole $\tau$ coordinate, when compared to those relative to the substituted bipyrroles. In particular, at the RHF/6-31G** level, the **BP** anti-planarization energy amounts to only 0.70 kcal/mol, while it is about three times and seven times as large for the **33′-MBP** and **NN′MBP** systems, respectively. As expected, the unsubstituted bipyrrole presents an energy maximum in the perpendicular conformation ($\tau = 90°$), which corresponds however to a lesser energy destabilization (2.25 kcal/mol) than that found for the synperiplanar conformation (3.56 kcal/mol). The other resulting energy minimum occurs close to $\tau = 135°$. The

(28) Glaser, R.; Horan, C. J. *Can. J. Chem.* **1996**, *74*, 1200.
(29) Scott, R. A.; Sheraga, H. A. *J. Chem. Phys.* **1966**, *45*, 2091.
(30) Mirsky, K. *Computing in Crystallography*; Proc. Int. Summer School in Crystallographic Computing; Delft University Press: Twente, 1978.
(31) Spackman, M. A. *J. Chem. Phys.* **1986**, *85*, 6579.
(32) Gordon, R. G.; Kim, Y. S. *J. Chem. Phys.* **1972**, *56*, 3122.
(33) Kim, Y. S.; Gordon, R. G. *J. Chem. Phys.* **1974**, *60*, 1842.
(34) The $\zeta = 1.24$ parameter set was used for the hydrogen atom.
(35) Bonati, L.; Moro, G.; Pitea, D.; Gatti, C. *J. Mol. Struct. THEOCHEM* **1990**, *208*, 235.
(36) Spackman, M. A. *J. Chem. Phys.* **1986**, *85*, 6587.
(37) Spackman, M. A.; Weber, H. P.; Craven, B. M. *J. Am. Chem. Soc.* **1988**, *110*, 775.
(38) Cheeseman, J. R.; Carroll, M. T.; Bader, R. F. W. *Chem. Phys. Lett.* **1988**, *143*, 450.
(39) Bader, R. F. W.; Chang, C. *J. Am. Chem. Soc.* **1989**, *93*, 2946 and 5095.
(40) Gatti, C.; Ponti, A.; Gamba, A.; Pagani, G. *J. Am. Chem. Soc.* **1992**, *114*, 8634.
(41) Frisch, M. J.; Trucks, G. W.; Schlegel, H. B.; Gill, P. M. W.; Johnson, B. G.; Robb, M. A.; Cheeseman, J. R.; Keith, T. A.; Petersson, G. A.; Montgomery, J. A.; Ragavachari, K.; Al-Laham, M. A.; Zagrewski, V. G.; Ortiz, J. V.; Foresman, J. B.; Cioslowski, J.; Stefanov, B. B.; Nanayakkara, A.; Challacombe, M.; Peng, C. Y.; Ayala, P. Y.; Chen, W.; Wong, M. W.; Andres, J. L.; Replogle, E. S.; Gomperts, R.; Martin, R. L.; Fox, D. J.; Binkley, J. S.; Defrees, D. J.; Baker, J.; Stewart, J. P.; Head-Gordon, M.; Gonzalez, C.; Pople, J. A. *GAUSSIAN 94* (Revision A.1); Gaussian Inc., Pittsburgh, PA, 1995.
(42) *PROAIM*; McMaster University: Ontario, Canada 1997.

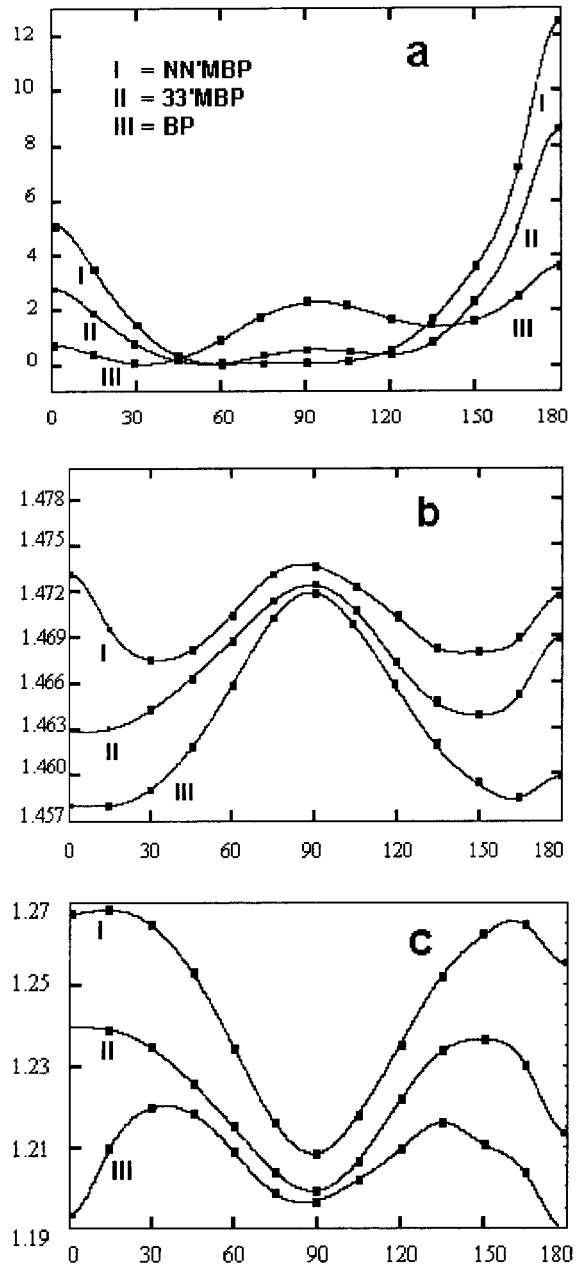


**Figure 1.** Bipyrroles, RHF/6-31G** model. Evolution, as a function of $\tau$, of (a) the relative energy (kcal/mol), (b) the interannular (C2−C2′) bond length (Å), and (c) bond order.

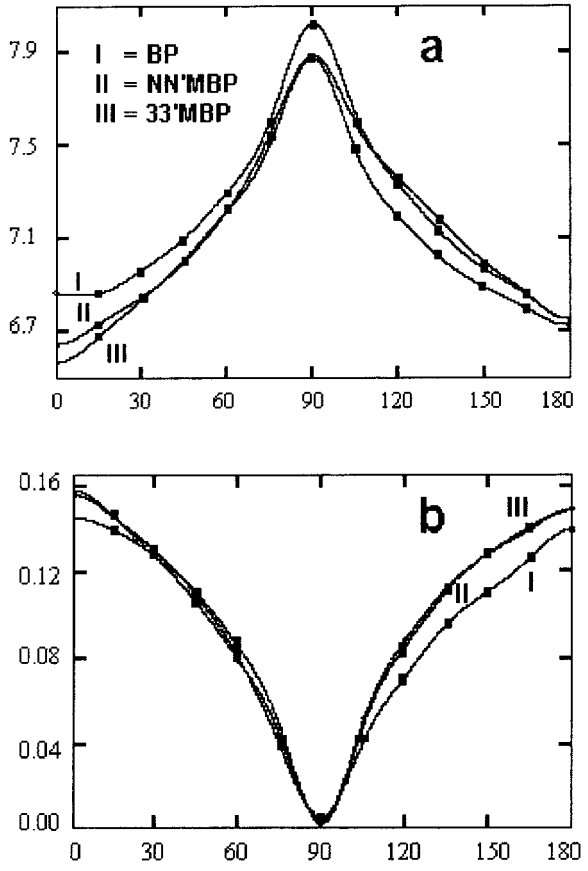


**Figure 2.** Bipyrroles, RHF/6-31G** model. Evolution, as a function of $\tau$, of (a) the ionization potential (eV) and (b) the interannular (C2−C2′) bond ellipticity

minor energy difference (1.55 kcal/mol) between the antiperiplanar and the perpendicular conformation is further lowered to 0.24 kcal/mol at the MP2/6-31G* level. Steric effects due to methyl substitution flatten the potential curve over the $\tau = 45-135°$ region in the **33′MBP** and **NN′MBP** derivatives. In the former compound the energy maximum corresponding to the perpendicular conformation is five times smaller than that in the electronically favored antiperiplanar conformation and this maximum nearly vanishes in **NN′MBP**. In these uncharged substituted bipyrroles the destabilizing steric effects appear to be largely dominant over the stabilizing $\pi$-electron delocalization mechanisms. Inspection of Figure 1b,c strengthens this observation. Interannular bond length should decrease on moving from the perpendicular to the antiperiplanar conformation as a result of the parallel increase in the interannular $\pi$-conjugation. Steric interactions may oppose such bond length reduction and either a less pronounced decrease or even the appearance of a minimum bond length at a torsion angle greater than zero, may occur. Figure 1b shows that bipyrroles have interannular bond lengths differing by less than 0.003 Å in their perpendicular conformations, with **NN′MBP** and **BP** exhibiting, respectively, the longest and the shortest distance. Such a trend is also found at $\tau = 0°$, but with a much broader spectrum (0.015 Å) for the interannular bond lengths. In particular, while **BP** and **33′MBP** systems, display nearly constant bond lengths in the $\tau = 0-15°$ range, the *N*-methyl- substituted compound shows a depth minimum for the interannular bond length at about $\tau = 30°$. This minimum is then followed by a drastic bond-length increase as torsion angles decrease, up to a maximum occurring at $\tau = 0°$ and with a bond length value (1.473 Å) equaling that of the perpendicular conformation. The shape of the associated bond order curves displayed in Figure 1c is, as expected, strictly specular to interannular bond length behavior.

**Ionization Potentials and Transition Energies.** Table 2 shows that the replacement of a hydrogen with a methyl group in pyrroles lowers the ionization potential (IP), substitution at C3 being more efficient than N-substitution. In the case of bipyrroles, the increasing loss of planarity in the **BP**, **33′MBP**, and **NN′MBP** series, adversely affects the positive contributions expected from substituents and a corresponding IP increase is observed along such a series. This behavior is clearly illustrated in Figure 2a, where Koopmans' estimates of the bipyrroles' IPs are displayed as a

**Table 2. Theoretical vs Experimental Vertical Ionization Potential (IP) and $\pi-\pi^*$ Transition Energies in Pyrroles and Bipyrroles**

| | IP (eV) | | | | $\pi-\pi^*$ transition energies (nm) | | |
|---|---|---|---|---|---|---|---|
| system | $-\epsilon_{HOMO}$ | $\Delta E(M)_{ROHF}$[a] | $\Delta E(M)_{UHF}$[a] | exp[b,c] | $\epsilon_{LUMO} - \epsilon_{HOMO}$ | CIS[d] | exp[b] |
| **P** | 7.96 | 8.19 | 6.82 | 0.90 | 91.2 | 168.3 | 205 |
| **NMP** | 7.88 | 6.90 | 7.03 | 0.80 | 92.9 | 171.5 | 210 |
| **3MP** | 7.84 | 6.85 | 6.57 | 0.67 | 91.4 | 168.5 | 210 |
| **BP** | 6.98 | 6.33 | 5.94 | 0.03 | 109.5 | 207.2 | 278 |
| **NN′MBP** | 7.23 | 6.49 | 6.14 | 0.30 | 104.5 | 194.8 | 250 |
| **33′MBP** | 7.14 | 6.36 | 6.03 | 0.08 | 103.6 | 193.3 | 257 |

[a] $\Delta E(M)_{ROHF} = E_{ROHF}(M^+) - E(M)_{RHF}$; $\Delta E(M)_{UHF} = E_{UHF}(M^+) - E(M)_{RHF}$ see text. [b] Reference 12. [c] Oxidation peak potential (vs Ag/$AgClO_4$ 0.1 M); for a proper comparison with theoretical IPs, see text. [d] 6-31G** and 6-31G* basis sets (on RHF/6-31G** geometry) were used for pyrroles and bipyrroles, respectively.

function of $\tau$. Indeed, the IP values exhibit the same order found for pyrroles, for any value of the $\tau$ twisting angle and even with an increased methyl substitution effect at $\tau = 0°$. However, when IP data are compared at the bipyrroles' minimum energy conformations, the smaller twisting angle of **BP** largely compensates the favorable electronic contributions operating in **33′MBP** and **NN′MBP**.

An approximately linear correlation ($R = 0.986$) between theoretical IPs (Koopmans' estimate) and the experimental[12] oxidation peak potentials is expected[13,43,44] and found.[45] Less meaningful results are obtained when the experimental data are regressed against $\Delta E_{UHF}$ ($R = 0.960$)[46] and especially $\Delta E_{ROHF}$ ($R = 0.817$), although this latter correlation greatly improves ($R = 0.995$)[47] if the **P** datum is omitted; regression against $\Delta E_{ROMP2}$ or $\Delta E_{UMP2}$ are not reported because they turn out to be not significant. Oxidation peak potentials (measured with respect to Ag/$AgClO_4$ 0.1 M, 0.34 V vs SCE) may be compared with theoretical IP estimates on an absolute scale only when a proper scale shift, adjusting gas-phase IP values to solid-state values and relating SCE to vacuum, is adopted.[13] Using the value (6.64 eV for Ag/$AgClO_4$ 0.1 M) suggested by Brédas et al.,[13] satisfactory agreement between experiment and theory is obtained, with experimental data lying between Koopmans' and the $\Delta E_{UHF}$ estimates.

The $\epsilon_{LUMO} - \epsilon_{HOMO}$ estimate of $\pi-\pi^*$ transition energies (Table 2) is indeed very crude. Better results are obtained from the CIS estimate, although they are still far from experimental results[12] because of the single-excitation approximation. However both CIS and $\epsilon_{LUMO} - \epsilon_{HOMO}$ values show an appreciable linear correlation with experimental data ($R = 0.993$ and $R = 0.991$, respectively).[48]

**Interannular Bond Orders and Ellipticities.** Figure 2b shows that all bipyrroles have an appreciable bond ellipticity at $\tau = 0°$, the largest value ($\epsilon = 0.158$) occurring for **33′MBP**. This value may be compared with the values found in *trans*-butadiene ($\epsilon = 0.071$), using the same basis set. As expected from simple symmetry considerations, the interannular bond ellipticities decrease monotonically as twisting angles increase, reaching their minimum value at $\tau = 0°$ and presenting specular behavior with respect to the IP trends. However, the calculated values for the interannular bond lengths, BCP densities, and bond orders suggest that this bond retains a significant amount of double-bond character (>20%) in bipyrroles, at any torsion angle value. This is also true at $\tau = 90°$, where the interannular $\pi$-conjugation is broken. The same behavior was found for polyacetylene oligomers by Brédas et al.,[15] who interpreted it in terms of a stabilizing and permanently active strong coupling between the $\pi$-framework of one subunit with the $\sigma$-framework of the other subunit and vice versa.

**Conformations and Planarization Energies in Bipyrrole Cations.** The investigation of torsion potentials for charged bipyrroles is also of importance as far as conducting properties of organic polymers are concerned. Indeed, the doping process—involving the presence of charges on the polymer chain—leads to local geometry relaxation from an aromatic toward a quinoid structure. The appearance of a quinoid structure implies a shortening of the interannular bond, which acquires a strong double-bond character and enhanced electronic stabilization of local chain planarity.[14] The most stable conformations for positively (+1) charged bipyrroles (UHF/6-31G** results) occur at $\tau = 24.6°$ for **NN′MBP** and at $\tau = 0.0°$ for **BP** and **33′MBP** (Figure 3a). Their perpendicular conformations, corresponding to their single energy maxima, turn out to be largely destabilized, lying, respectively, 19, 17, and 14 kcal/mol above their energy minima. As expected, the achievement of quinoid structures in the positively charged bipyrroles significantly shortens the interannular bond, from 1.460, 1.469, and 1.471 Å in **BP**, **33′MBP**, and **NN′MBP** to 1.390, 1.393, and 1.400 Å in their corresponding cations, evaluated at their minimum energy conformations. Accordingly, the interannular bond orders increase, respectively, from 1.26, 1.21, and 1.21 to 1.62, 1.59, and 1.55. Figure 3b shows that only the **NN′MBP** cation exhibits a minimum bond length at a $\tau$ value significantly different from zero. As expected, this minimum occurs in very close correspondence to the energy minimum.

The results so far discussed allow for a description of the effect of methyl substitution on pyrroles and for a simple understanding of how these effects are adversely affected by twisting in the corresponding bipyrroles. However, some questions remain unexplained. For instance, why is methyl substitution at C3 more efficient than at nitrogen, in determining favorable electronic properties in pyrroles and bipyrroles? Moreover, what are specifically the dominant steric effects which in-

(43) Miller, L. L.; Nordblom, G. D.; Mayeda, E. A. *J. Org. Chem.* **1972**, *37*, 916.
(44) Parker, V. D. *J. Am. Chem. Soc.* **1974**, *96*, 5656.
(45) Slope: 1.14 ± 0.10. Intercept: 6.98 ± 0.06.
(46) Slope: 1.15 ± 0.17. Intercept: 5.89 ± 0.10.
(47) Slope: 0.78 ± 0.05. Intercept: 6.29 ± 0.02.
(48) $R = 0.993$, slope 0.54 ± 0.03, intercept 57 ± 8; $R = 0.991$, slope 0.26 ± 0.02, intercept 38 ± 4.

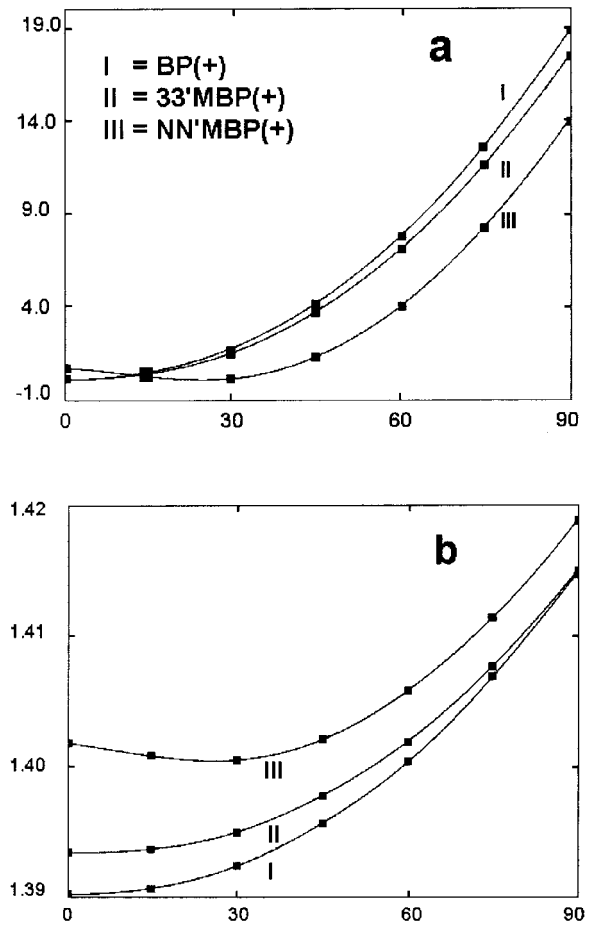


**Figure 3.** Bipyrrole cations, UHF/6-31G** model. Evolution, as a function of $\tau$, of (a) the relative energy (kcal/mol) and (b) the interannular (C2−C2′) bond length (Å).

crease the anti-planarization energy in **NN′MBP** so much with respect to **33′MBP**? The AIM approach may help us find an answer to these two questions.

**Site vs Electronic Efficiency of Methyl Substitution.** Methylation allows for an increased release of the nitrogen lone pair to the conjugated system with a parallel increase in C−N bond ellipticity, compared to the **P** ($\epsilon$ = 0.153). This mechanism is slightly more efficient in **NMP** ($\epsilon$ = 0.177) than it is in **3MP** ($\epsilon$ = 0.171). However C3-methylation also involves a clear enhancement of the C2−C3 bond ellipticity (from 0.396 in **P** to 0.415 in **3MP**) and a stronger hyperconjugative coupling of the $\pi$-type orbitals of the methyl group with the $\pi$ system in the aromatic ring. The latter effect is revealed by comparing the X−$CH_3$ (X = C, N) ellipticities and bond orders in **NMP** [$\epsilon$(N−$CH_3$) = 0.021; $n$ = 0.96] with those in **3MP** [$\epsilon$(C3−$CH_3$) = 0.036; $n$ = 1.08]. The chemical significance of the reported ellipticity and bond order data may be better appreciated when they are related to the corresponding values for suitably chosen reference systems (see note 49).

A quantitative insight on the charge density rearrangements caused by methyl substitution on **P** is given in Table 3, where the methyl-induced changes in the $\sigma$, $\pi$ and total atomic electron population are reported. The modest deviations from ring planarity occurring in **3MP** and **NMP** allowed for such a symmetry partitioning of the atomic populations. Methyl substitution involves a small charge transfer to the ring (0.07 and 0.10 electron charges in **3MP** and **NMP**, respectively), as a result of a large increase in the ring $\pi$ electron population (1.087 and 0.632) and a concomitant similar decrease in its $\sigma$ population (−1.017 and −0.532). This opposed flux of electrons is about twice as big in **3MP** as it is in **NMP**, since the release of charge to the ring from the $\pi$-type orbitals of the methyl group is far more efficient in the case of C3-substitution. Table 3 shows that only 0.494 $\pi$ electron charges are left on methyl in **3MP**, compared with the corresponding value of 1.617 for **NMP**. Furthermore, while the increase in the $P^{\pi}$ ring population in **NMP** is mainly due to an augmentation in the $\pi$-electron population at nitrogen, in **3MP** a major transfer of $\pi$ electrons to the C2-type atoms and a partial $\pi$-electron removal from the C3-type atoms also occurs. This mechanism yields a greater equalization of the ring atom $\pi$ electron populations in **3MP** than in **NMP**. Overall, this increased $\pi$-electron delocalization in **3MP**, further enhances the positive effect of the augmented ring $\pi$ population afforded by methyl substitution.

**Table 3. Charge Rearrangements in Methyl-Substituted Pyrroles**

| system | $P^a$ | Ω ring | N | C2 | C5 | C3 | C4 | $CH_3{}^b$ |
|---|---|---|---|---|---|---|---|---|
| **P** | $P^{\pi}$ | 5.295 | 1.213 | 0.829 | | 1.212 | | |
| **NMP** | $P^{\pi}$ | 5.927 | 1.971 | 0.863 | | 1.115 | | |
| | $\Delta P^{T}$ | 0.100 | 0.090 | 0.000 | | 0.005 | | 8.421 |
| | $\Delta P^{\sigma}$ | −0.532 | −0.668 | −0.034 | | 0.102 | | 6.804 |
| | $\Delta P^{\pi}$ | 0.632 | 0.758 | 0.034 | | −0.097 | | 1.617 |
| **3MP** | $P^{\pi}$ | 6.382 | 1.884 | 1.227 | 1.221 | 1.041 | 1.009 | |
| | $\Delta P^{T}$ | 0.070 | 0.002 | 0.014 | −0.005 | 0.047 | 0.012 | 8.961 |
| | $\Delta P^{\sigma}$ | −1.017 | −0.669 | −0.384 | −0.397 | 0.218 | 0.215 | 8.467 |
| | $\Delta P^{\pi}$ | 1.087 | 0.671 | 0.398 | 0.392 | −0.171 | −0.203 | 0.494 |

[a] $\Delta P^{T}$, $\Delta P^{\sigma}$, and $\Delta P^{\pi}$ are, respectively, the total, $\sigma$- and $\pi$-electron population *changes* following methyl substitution. [b] The $\Delta P^{x}$ (x = T, $\sigma$, $\pi$) values for the −$CH_3$ group are the corresponding $P^{x}$ electron populations.

The topological properties (Supporting Information) of bipyrroles, at their optimum geometries, are similar to those found for the corresponding pyrroles, apart from a significant enhancement of the N1−C2 (N1′−C2′) ellipticities. The higher torsion angles in the methyl-substituted derivatives yield smaller interannular bond ellipticities (see above) and overlaps with neighboring bonds, compared to **BP** (the $O_{123}$ values being 0.955, 0.866, and 0.864 in **BP**, **NN′MBP**, and **33′MBP**, respectively). When the antiperiplanar conformations are considered, the $O_{123}$ values approach the value of one and interannular bond ellipticities increase, while those of the remaining bonds generally decrease, due to the $\pi$-electron flow from the ring bonds into the interannular bond. The topological properties of bipyrroles comply with the trends found for ionization potentials. At $\tau$ = 0° the methyl-substituted compounds exhibit higher interannular bond ellipticities and lower ionization potentials than **BP**; the reverse being true when the same quantities are compared at the geometry of the most stable conformations for such systems.

(49) For the sake of comparison, the RHF/6-31G** values of the C−C bond ellipticities (and orders) in ethylene, benzene, and propene (C−C formal single bond) are 0.448 (2.06), 0.231 (1.62), and 0.028 (1.09), respectively; the values of the C−N bond ellipticities (and orders) in methylenimmine and *N*-methylformilimine are 0.258 (1.96) and 0.020 (1.03), respectively.

**Table 4. Interaction Energies (kcal/mol) among Facing Atoms (See Text) in NN′MBP and 33′MBP[a]**

| system | $E_{es}$ | $E_{nb}^{GK}$ ($E_{int}$) | $E_{nb}^{LJ}$ ($E_{int}$) | $E_{nb}^{BU}$ ($E_{int}$) |
|---|---|---|---|---|
| **NN′MBP**, $\tau$ = opt | −10.8 | 2.2 (−8.6) | −1.4 (−12.2) | −0.4 (−11.2) |
| **NN′MBP**, $\tau$ = 0. | −0.8 | 15.0 (14.2) | −0.8 (−1.6) | 2.8 (2.0) |
| **33′MBP**, $\tau$ = opt | −32.8 | 2.0 (−30.8) | −1.4 (−34.2) | −0.4 (−33.2) |
| **33′MBP**, $\tau$ = 0. | −23.6 | 12.4 (−11.2) | −1.4 (−25.0) | 2.0 (−21.6) |

[a] $E_{nb}^{GK}$, $E_{nb}^{LJ}$, and $E_{nb}^{BU}$ are the nonbonding energies as derived from the Gordon−Kim, the Lennard-Jones, and the Buckingham models (see text), respectively. The corresponding total interaction energies ($E_{int}$) are reported in parentheses.

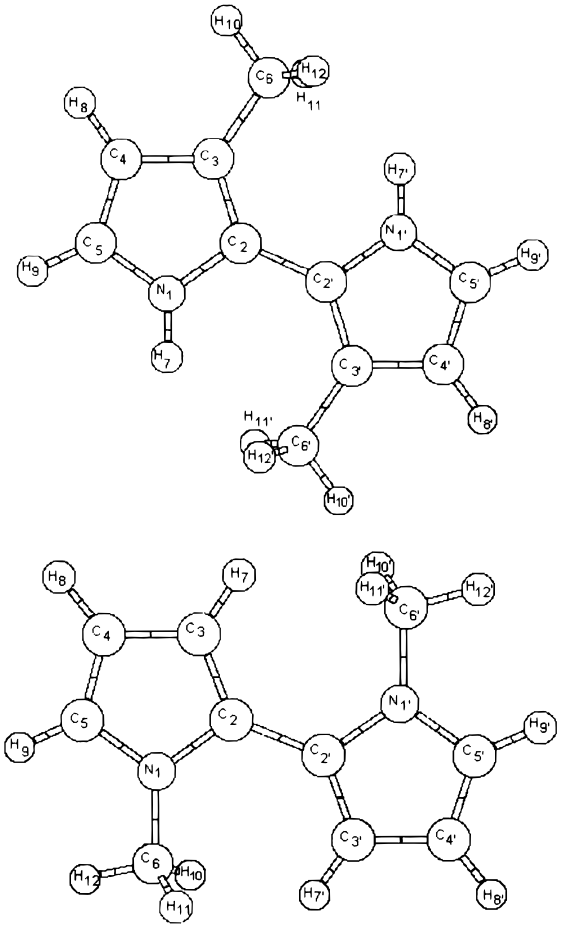


**Figure 4.** Optimized structure (RHF/6-31G**, $\tau$ = 0) and atomic numbering of (top) **33′MBP** and (bottom) **NN′MBP**.

**Intramolecular Interaction Energies in 33′MBP and NN′MBP.** Table 4 details, as a function of $\tau$, the electrostatic and nonbonding contributions to the interaction energy, among facing atoms in **33′MBP** and **NN′MBP** systems. In the case of the former compound (Figure 4) we considered the interactions of set *A* {N1, H7} atoms on one ring with set *B*′ {C3′, C6′, H11′, H12′} atoms on the other ring, and the corresponding interactions among the atoms of the symmetry related *A*′,*B* sets; for **NN′MBP**, set *A* included N1, C6, H10, H11 atoms and set *B*′ included C3′, H7′ atoms. In the following discussion, the nonbonding and the total interaction energies derived from the Gordon−Kim, the Lennard-Jones, and the Buckingham models are referred to as ($E_{nb}^{GK}$, $E_{int}^{GK}$), ($E_{nb}^{LJ}$, $E_{int}^{LJ}$), ($E_{nb}^{BU}$, $E_{int}^{BU}$), respectively. Table 4 shows that, independently of the model chosen for $E_{nb}$, both systems are stabilized by the facing atom interactions when the minimum energy conformations ($\tau$ = opt) are considered. However, in the case of **33′MBP** these interactions are, at $\tau$ = 0, far less stabilizing ($E_{int}^{GK}$ = −11.2 kcal/mol) than at $\tau$ = opt ($E_{int}^{GK}$ = −30.8 kcal/mol). For **NN′MBP**, these interactions are even destabilizing at $\tau$ = 0 (except in the case of the $E_{int}^{LJ}$ estimate that once again predicts a very small energy stabilization for it). While the two systems are similarly affected by the nonbonding contributions to their facing atom interaction energies (both at $\tau$ = 0 and at $\tau$ = opt), they turn out to be strongly differentiated by their electrostatic contributions. $E_{es}$ amounts to −23.6 kcal/mol in **33′MBP** and just −0.8 kcal/mol in **NN′MBP**, at $\tau$ = 0°. Closer examination of the individual contributions to $E_{es}$ in **33′MBP** and **NN′MBP** shows that the large differences found in their electrostatic energies may be easily explained. Indeed, **33′MBP** is characterized by globally more favorable electrostatic interactions of the N1 (N1′) atom with the C3′ (C3) atom and with the facing methyl group on the other ring (−6.9, −10.8 kcal/mol) when compared to the interactions of the N1 (N1′) atom or of its linked methyl group with C3′ (C3) in **NN′MBP** (−14.5 and +6.9 kcal/mol). The electrostatic energy difference between **33′MBP** and **NN′MBP**, arising from these selected atomic interactions, amounts to −20.8 kcal/mol [ (−17.7 − (−)7.6) × 2] and accounts for over 88% of the total $E_{es}$ difference. The electrostatic contributions due to the interactions involving H7 (H7′) atoms of one ring with facing atoms on the other ring are, on the other hand, similar and destabilizing both in **33′MBP** (5.8 kcal/mol) and in **NN′MBP** systems (7.2 kcal/mol).

The $E_{int}$ values predicted by the three nonbonding energy models largely differ among themselves (in particular $E_{int}^{GK}$ vs $E_{int}^{LJ}$, $E_{int}^{BU}$) as a result of quite different estimates for the corresponding nonbonding energies. As far as this discrepancy is concerned, Spackman[31] has pointed out that Gordon−Kim potentials are always more repulsive than any experimentally derived potential, because these latter generally include a large attractive component which arises from neglect of a large electrostatic component of the energy in their derivations. The inclusion of an electrostatic term in the evaluation of $E_{int}$ (eqs 1 and 2) may therefore be questionable when experimentally derived nonbonding potentials are adopted. However, it is gratifying that the three models give similar predictions for the $\Delta\delta$ difference

$$\Delta\delta = \Delta_{NN'MBP} - \Delta_{33'MBP} = [E_{int}(\tau = 0°) - E_{int}(\tau = \text{opt})]_{NN'MBP} - [E_{int}(\tau = 0°) - E_{int}(\tau = \text{opt})]_{33'MBP}$$

between the interaction energy changes ($\Delta$) for **NN′MBP** and **33′MBP** on passing from $\tau$ = 0° to $\tau$ = opt. The value of $\Delta\delta$ amounts to 3.2, 1.4, and 1.6 kcal/mol for the $E_{int}^{GK}$, $E_{int}^{LJ}$, and $E_{int}^{BU}$ models, respectively. These values compare favorably with the corresponding difference found for the RHF/6-31G** planarization energies (2.4 kcal/mol, Table 1). Quite obviously, the absolute values of the interaction energy changes ($\Delta_{NN'MBP}$ or $\Delta_{33'MBP}$) may not be directly compared with the RHF planarization energies. Indeed, these $\Delta$ values do not take into account the $\pi$-electron delocalization energy increase which is achieved when the torsion angle decreases.

**Comparison with Previous Theoretical and Experimental Studies.** The use of a better quality basis set and of a fully geometrical optimization procedure (thanks to the improved present-day computational facilities) yields RHF theoretical predictions which differ somewhat from those previously found.[14] For instance, our computations predict a non-coplanar conformation for **BP**, with an absolute energy minimum occurring at a torsion angle noticeably different from zero (32.8°) and with an evident secondary minimum at $\tau = 135°$. In the previous work by Brédas et al. a single-energy minimum was found, corresponding to the coplanar conformation. Our perpendicular conformation is only 1.5 kcal/mol (or even as low as 0.24 kcal/mol at the MP2/6-31G*//RHF/6-31G** level) higher in energy than the coplanar conformation, to be compared with the corresponding value of 4 kcal/mol reported in ref 14. The predicted torsion angles for **33′MBP** and **NN′MBP** (52.3, 59.6) are somewhat larger than those found by Brédas et al.[14] for the $C_2$ symmetry **33′MBP** and 1-methyl-2,2′-bipyrrole (37.7°, 51.5°) systems. Indeed, our calculations yield an extremely flat potential curve (Figure 1a), in the $\tau = 45-135°$ range for these two systems. This result agrees both with the crystal structure[50] of **33′MBP**, which presents two distinct molecules characterized by twisting angles of 55° and 110°, and with the crystal structure[50] of all-α-*N*-methyltetrapyrrole, also characterized by two distinct molecules, one with similar angles between consecutive rings of the order of 50°, and the other with angles ranging from 50° to 66°. Our predicted planarization energies for **NN′MBP** and **33′MBP** (5.15 and 2.74 kcal/mol) are about one-third of those reported in ref 14, although their ratio (1.9) does not substantially differ from the previous estimate (2.5).

The values found for interannular bond length in **BP** and **NN′MBP** are only slightly higher (1.460, 1.471 Å) than those derived (1.448, 1.461 Å) from X-ray diffraction experiments.[50] The substantial ellipticities of these bonds in bipyrroles (Figure 2b) point out their $\pi$-bonding character, which is indeed remarkable at $\tau = 0°$, and not negligible even in the noncoplanar minimum energy conformations. However, as the perpendicular conformations of bipyrroles still exhibit (Figure 1c) a significantly high value for the interannular bond order (∼1.2), the dominant role of the C−C $sp^2-sp^2$ interactions in determining such a bond-order enhancement (relative to a normal single bond), seems evident. This result confirms a previous observation by Brédas et al.[14]

## Conclusions

The results of this research (Parts I and II) have brought the long-debated question of the different effects on spectral and electrical properties of a polypyrrole chain produced by the presence of methyl groups either on the nitrogen atom or on the $\beta$ carbons to a more mature level of comprehension.

Our theoretical investigation shows that the replacement of a hydrogen atom with a methyl group in pyrroles lowers the ionization potential (IP), with substitution at C3 being more efficient than N-substitution. The increasing loss of planarity in the **BP**, **33′MBP**, and **NN′MBP** series, adversely affects the positive contributions expected from methyl substitution, and a corresponding increase in IP is observed along the series, in agreement with the experimentally determined parallel increase in oxidation peak potentials. The higher IP and oxidation peak potential for **NN′MBP** as compared to **33′MBP** is the result of both the slightly larger torsion angle of the equilibrium conformation of the former and of the higher electronic efficiency of C-3 substitution as opposed to N-substitution in pyrroles.

This study also provides interesting insights as to why methyl substitution at C3 is more efficient than at N in transmitting electronic effects to the pyrrole ring and also as to what are the dominant effects which so greatly increase the anti-planarization energy in **NN′MBP** as compared to **33′MBP**.

It was demonstrated that methyl substitution on the pyrrole ring increases $\pi$- and decreases $\sigma$-electronic populations on the ring. This opposite flux of electrons is twice as great in **3MP** as it is in **NMP**. In **NMP**, the $\pi$ population mostly augments at N, while in **3MP** $\pi$ population also increases at C2 and C5. Overall, C-substitution is more efficient than N-substitution—as judged by electrochemical oxidative potentials—owing to the more efficient release of $\pi$ population to the ring and to the related enhanced equalization of $\pi$-electron populations on the ring's atoms.

Evaluation of intramolecular interaction energy among facing atoms reveals that both **33′MBP** and **NN′MBP** are stabilized by these atomic interactions at their minimum energy conformation. These interaction energies are significantly lowered at $\tau = 0°$ for **33′MBP** and become even destabilizing in the case of **NN′MBP**. The greater anti-planarization energy of **NN′MBP**, as compared to **33′MBP**, is due to the larger decrease in the stabilizing electrostatic contribution and to the larger increase in the non bonding contribution, which occurs at $\tau = 0°$ in the former.

The use of a better quality basis set and of complete geometry optimizations has led to significant changes in the computed conformations of bipyrroles and in the shape of their potential energy curves, as compared to what had previously been reported in the literature.[14] For instance, we found a nonplanar conformation for **BP** ($\tau = 32.8°$) to which a planar conformation had formerly been assigned and an extremely flat potential curve, in the $\tau = 45-135°$ interval, for both **33′MBP** and **NN′MBP**. We demonstrated how the increased flatness of our curves, as opposed to those previously published,[14] is the result of a balance between the steric effects which favor the noncoplanar conformations and the $\pi$-electron delocalization mechanisms which stabilize the coplanar ones.

Calculations also give very interesting results in the case of the monocations derived from **NN′MBP** and **33′MBP.** While the **33′MBP** and **BP** cations adopt an anti-coplanar conformation, the most stable conformation for the **NN′MBP** cation is the one exhibiting an ∼25° torsional angle. Our computed anti-planarization energy of the **NN′MBP** cation is however very small (0.6 kcal/mol), as compared to the anti-planarization energies for the **NN′MBP** and **33′MBP** neutral systems and to their estimated difference (2.5−3.5 kcal/mol). It is well-known that the doping process, which injects charges on the polymer chain, leads to local geometry

(50) Street, G. B. *Handbook on Conducting Polymers*; Skotheim, Ed.; Marcel Dekker: New York, 1985.

relaxation from an aromatic to a quinoid structure. The appearance of a quinoid structure implies significant shortening of the interannular bond, which acquires a strong double-bond character, and enhanced electronic stabilization of local chain planarity.[14] Our estimate of such bond shortening in bipyrrole cations is about 0.07 Å for all the systems we investigated, thus confirming that these relaxation mechanisms are active.

It has been proposed[14] that the significantly smaller maximum conductivities which have been achieved so far in doped poly(*N*-methylpyrrole) as opposed to doped poly(3-alkylpyrrole) are at least in part due to the greater difficulty for the chains of the former to become coplanar. According to this view, the intrachain mobility of the charge carriers in doped poly(*N*-methylpyrrole) should be lower and the conductivity significantly smaller. However, the first part of our study has demonstrated[12] that the use of monomers which allowed us to obtain defect-free materials, and the adoption of fine-tuned, identical experimental conditions in the electrochemical anodic oxidation process, afforded quite similar conductivities for **poly(NN′MBP)** and **poly-(33′MBP)**, despite the great difference in the anti-planarization energy of the corresponding neutral monomers. Thus, one might infer that the greater or lesser difficulty in achieving local chain planarity in doped polypyrroles should be more closely correlated to the anti-planarization energies of the charged monomers rather than to the anti-planarization energies of the neutral monomers. Alternatively, one might suppose that under our experimental conditions, the lower intrachain mobility of charge carriers in **poly(N-N′MBP)** as compared to **poly(33′MBP)** is compensated for by some unknown mechanism which greatly enhances the interchain mobility of the former. Which of these two factors plays the dominant role, cannot be deduced through the present study.

**Acknowledgment.** The work was supported in part by CNR.

**Supporting Information Available:** Listing (Tables 5 and 6) of bond lengths and topological bond properties for the investigated pyrroles and bipyrroles at their RHF/6-31G** optimized geometries and at their RHF/6-31G** optimized antiperiplanar ($\tau = 0$) conformations. This material is available free of charge via the Internet at http://pubs.acs.org.

CM000092R